Twin Motor Drives in Weapon Systems

JIRI BALLA
Department of weapons and ammunition
University of Defence
Kounicova 65, 662 10 Brno
CZECH REPUBLIC
jiri.balla@unob.cz http://www.unob.cz

Abstract: - The paper deals with the use of the twin motor drives in loading systems of guns and in small arms. The mechanical parts are described as systems with three degrees of freedom connected with flexible coupling. The electrical and hydraulic parts enable to determine the main power characteristics as are the torque and the angular velocity driving the ramming device and the chain gun mechanism.

Key-Words: - Twin motor, Chain gun, Gatling gun, Electric DC drive, Loading system, Ramming device, Motion equation.

1 Introduction

Modern howitzers, tank gun and mortars are distinguished by the increase of the maximum range, the effect on the targets and the hit probability.

The increase of the hit probability can be achieved also by the increase of the rate of fire, now by firing of Multiple Rounds Simultaneous Impact (MRSI) effects, for example. One of the tasks which must be completed is cartridge loading since the rate of fire depends on the loading velocity. The MRSI effect is achieved by the coordination of loading system with other gun systems – breech, aiming, fire control system (FCS) etc.

One of the tasks which must be completed is cartridge loading since the rate of fire depends on the loading velocity.

The gun loading is a very difficult operation from the viewpoint of energy consumption by a gun crew.

It follows from the following reasons.

The loading work for one round approx 150mm calibre is 2800 J. The human power is limited to 120 W. The lengths of the cartridges are until 1 m and the mass from 15 to 50 kg as shown in [3] or [9].

Ramming as one of the as one of the significant operation is very difficult mainly when loading by hand. Cartridge ramming is an operation which influences weapon reliability most importantly on a rapidity of fire and it belongs to the hardest thing before a shot.

The maximum rapidity of fire attainable during loading by hand is two rounds a minute.

A mechanization of cartridge ramming was the first step destined for an easement of the loading process.

The ramming can start if the breech is opened and the fired cartridge case is ejected from the barrel chamber and from the loading space. After complete ramming of a new cartridge (or its parts) can start following periods of the functional cycle (closing and locking of the barrel chamber and the shot). The ramming difficulties can be explained by means of Fig. 1 representing the forces acting against the projectile movement – see [3] and [8].

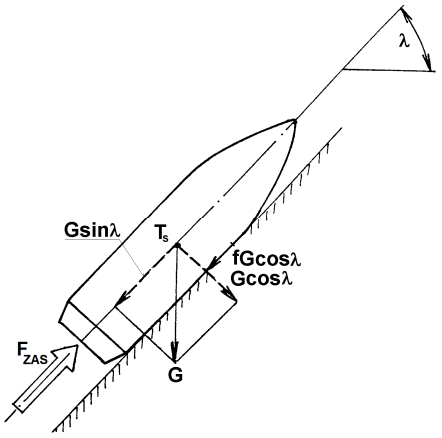

Fig. 1 Simplification of ramming resistance

To move the projectile, the ramming force F_{zas} according to the expression (1) has to be:

$$F_{zas} \rangle G\left(\sin\lambda + f\cos\lambda\right). \quad (1)$$

So the magnitude of the resistance against the ramming changes with the angle of elevation and for the calibre around 150mm it is approx. in limits from 85N to 412N without taking into consideration the resistances at the breech closing and the pressing the projectile into the forcing cone. With respect to this fact the man is able to produce the power 120W. The achievable ramming velocity may have been 0.3 $m.s^{-1}$ when resistances are 400N therefore. This could not be sufficient for reliable pressing of the projectile into the forcing cone and release of the extractors catching the breech. The total resistances against ramming for calibres projectiles 122 mm and 152 mm depending on the elevation angle λ are shown in Fig. 2.

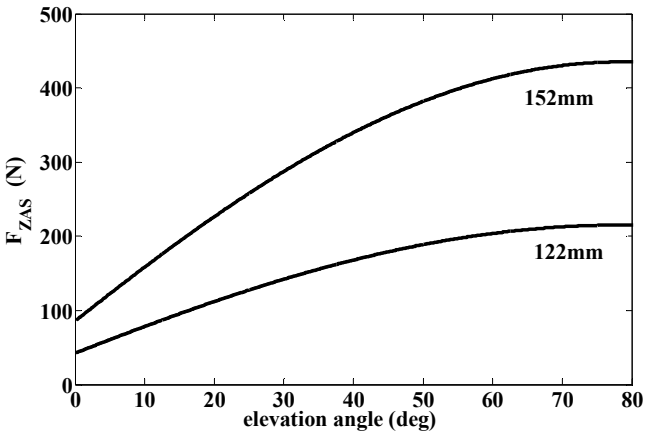

Fig. 2 Ramming resistance

In [3] and [8] there are given the recommended values of the ramming velocities at the end of movement when shell is engraved into the forcing cone, see Table 1.

Table 1 Ramming velocities

ramming velocity	v_{min} (m/s)	v_{max} (m/s)
unitary cartridge	0.6 – 1	4 – 6.5
separated cartridge	more than 0.3	1 – 1.4 (charges) 3 (projectiles)

The twin motor drives (or double motor equipments in other words) are used in many technical military applications as are externally powered automatic weapons (Gatling systems, chain guns) or loading systems of guns, see [1], [2], [6] and [7] for example. The reasons can be following: decreasing of whole inertia mass moment and improvement of dynamical properties of drives, location of drives into the limited space in combat vehicles, tanks or aircrafts. In any cases the velocity adjustment to achieve the required of rapidity of fire is possible.

Finally during malfunction of the one drive the second one is able to operate with decreased power. Only the two drives are usually used in weapon application in contradistinction to non-military area where more than two motors actuate the machine. The main issue of these drives follows from a proportional distribution of powers to each motor. The motors with hard characteristic have very unequal distribution of power in comparison with them having a soft characteristic. A redistributing of powers among individual drives can cause an overloading one of them and an inconsonance of angular velocities driving motors brings along a danger of an oscillating process.

The drives having the series excited DC motors will be discussed in the next paragraph. They are very often used in the weapons applications which are suitable due to they work in short time with longer breaks ensuring their cooling when they do not operate.

2 Twin electric drive in ramming device application

The often arrangement of the twin-motored drives using DC motors is represented in Fig. 3. The torques of both motors act on the first wheel in the transmission linking the gear box. The elastic shafts rotating with angular velocities $\dot{\varphi}_1, \dot{\varphi}_2$ have own torsion rigidities k_1, k_2, damping torsion coefficients b_1, b_2 and mass moments of inertia I_1, I_2. The driven part has the inertia mass moment symbolized by I_3. This part is being loaded by the M_Z load torque.

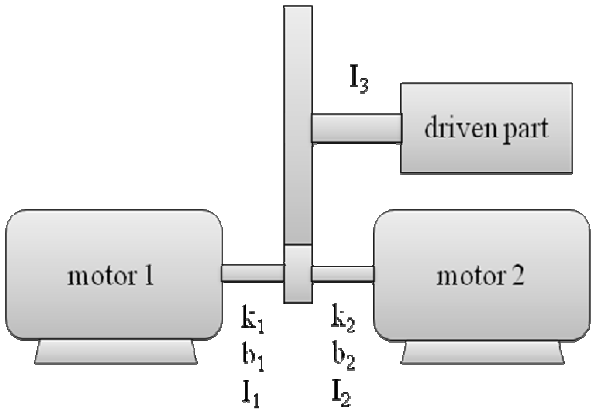

Fig. 3 Twin drive scheme

The mechanical part can be written using of the Lagrange equations of the second order:

$$\frac{\mathrm{d}}{\mathrm{d}t}\left(\frac{\partial E_\mathrm{K}}{\partial \dot{q}_\mathrm{j}}\right) - \frac{\partial E_\mathrm{K}}{\partial q_\mathrm{j}} = -\frac{\partial E_\mathrm{P}}{\partial q_\mathrm{j}} - \frac{\partial R_\mathrm{d}}{\partial q_\mathrm{j}} + Q_\mathrm{j}. \qquad (2)$$

The expression (2) describing the dynamic model with the three degrees of freedom has been determined as follows.

The kinetic energy of the system is:

$$E_\mathrm{K} = 0.5 I_1 \dot{\varphi}_1^2 + 0.5 I_2 \dot{\varphi}_2^2 + 0.5 I_3^{\mathrm{red}} \dot{\varphi}_3^2 \qquad (3)$$

where I_1 ... inertia mass moment of 1st motor shaft,

I_2 ... inertia mass moment of 2nd motor shaft,

I_3^{red} ... variable reduced inertia mass moment of the other part depending on the rammer mass.

The potential energy and dissipative function are given as:

$$E_\mathrm{P} = 0.5 k_1 \left(\varphi_3 - \varphi_1\right)^2 + 0.5 k_2 \left(\varphi_2 - \varphi_3\right)^2 \qquad (4)$$

where

k_1, k_2 – rigidities of the motor 1 and 2 shafts.

The dissipative function is

$$R_{\mathrm{D}} = 0.5b_1\left(\dot{\varphi}_3 - \dot{\varphi}_1\right)^2 + 0.5b_2\left(\dot{\varphi}_2 - \dot{\varphi}_3\right)^2 \qquad (5)$$

where

b_1, b_2 – damping factors in the linking between the motor shafts 1, 2 and gearbox.

The dissipative function is very often substituted by damping of every degree of freedom only by one force the same way as in [10] or [11].

The mechanical and electrical system is described with helping the Fig. 4 and following equations.

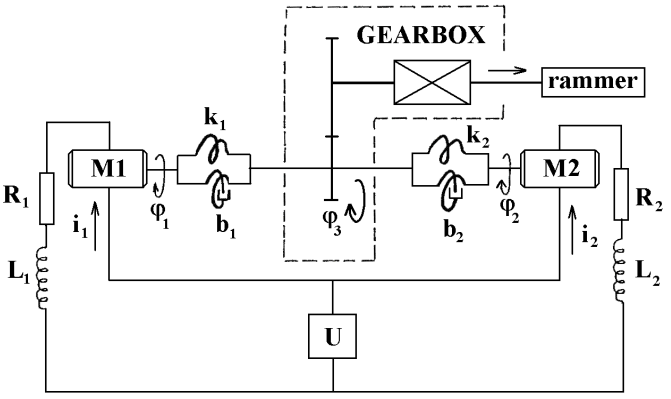

Fig. 4 Mechanical and electrical parts

The mechanical part equations follow from (2) and they can be written, see [11], [13] or [14]

$$I_1\ddot{\varphi}_1 = M_{\mathrm{M}_1} + k_1(\varphi_3 - \varphi_1) + b_1(\dot{\varphi}_3 - \dot{\varphi}_1), \qquad (6)$$

$$I_2\ddot{\varphi}_2 = M_{\mathrm{M}_2} - k_2(\varphi_2 - \varphi_3) - b_2(\dot{\varphi}_2 - \dot{\varphi}_3), \qquad (7)$$

$$I_3^{\mathrm{red}}\ddot{\varphi}_3 = 0.5\frac{\mathrm{d}I_3^{\mathrm{red}}}{\mathrm{d}\varphi_3}\dot{\varphi}_3^2 + k_2(\varphi_2 - \varphi_3) - k_1(\varphi_3 - \varphi_1) - b_2(\dot{\varphi}_2 - \dot{\varphi}_3) - b_1(\dot{\varphi}_3 - \dot{\varphi}_1) - M_{\mathrm{Z}}. \qquad (8)$$

The torques of motors are given

$$M_{\mathrm{M}_1} = K_{\mathrm{MS}_1} i_1^2, \qquad (9)$$

$$M_{\mathrm{M}_2} = K_{\mathrm{MS}_2} i_2^2, \qquad (10)$$

where K_{MS_1}, K_{MS_2} are the electromechanical constants.

The load torque is

$$M_{\mathrm{Z}} = F_{\mathrm{zas}} i_{\mathrm{G}}, \qquad (11)$$

where i_{G} is total transmission ratio from load to the part 3 representing of shaft having I_3 mass moment of inertia, gear box, rammer and projectile.

To determine the motors torques, the i_1, i_2 currents have to be set using the differential equations of the first order:

$$L_1\frac{\mathrm{d}i_1}{\mathrm{d}t} + R_1 i_1 + U_{\mathrm{b1}} = U, \qquad (12)$$

$$L_2\frac{\mathrm{d}i_2}{\mathrm{d}t} + R_2 i_2 + U_{\mathrm{b2}} = U \qquad (13)$$

where

U – supply voltage [V],

R_1, R_2 – resistance of armatures [Ω],

L_1, L_2 – inductance of armatures [H],

U_{b1}, U_{b1}– electromotive forces (emf) [V],

$$U_{\mathrm{b1}} = K_{\mathrm{ES}_1}\dot{\varphi}_1 i_1, \qquad (14)$$

$$U_{\mathrm{b2}} = K_{\mathrm{ES}_2}\dot{\varphi}_2 i_2, \qquad (15)$$

K_{ES_1}, K_{ES_2} – electromagnetic constants of both series excited motors.

Since equations describing the system are nonlinear they have to be solved numerically. The analytical solution is possible only in the several special cases as it is mentioned in [13], [14] and [15].

The system of the five differential equations (6), (7), (8), (12) and (13) has been solved using by the Runge-Kutta integration method of 4th order together with the other additional equations as it was used in [4] or [15].

The suitable integration step has been chosen as 0.0001s for the specific purpose. It corresponds to known condition between the minimal integration step and the maximal considered frequency $f_{\max}$ of the undamped system as it is recommended in [12] or [15] as well

$$\Delta t_{\min} = \frac{1}{\pi f_{\max}}. \qquad (16)$$

But in case of the mass moment of inertia change and during impacts the integration step has to be cut down hundred times.

The oncoming results have been gained with comparison of calculations and measurements on the medium calibre loading device [3] when the software was debugged.

3 Results of ramming device calculations

The results of calculation are presented onward. The numerical values of the input parameters belonging to the system were obtained from technical specifications and drawings. Due to very large numbers of inputs only the most important there are mentioned hereto. First of all, the significant values for the case when both motors have the identically characteristics, see Table 2.

The power supply voltage changes according to the instantaneous value of both currents and it is modelled by the equation

$$U = U_0 - k_{\mathrm{i}}\left(i_1 + i_2\right) \qquad (17)$$

where k_{i} is factor obtained from the technical experiments on the piece and depending on the instantaneous currents consumption when device operates. The variation of voltage during ramming time is drawn in the Fig. 5.

The inputs belonging to the electric drive were chosen according to design of the piece and they were corrected with respect to the technical experiments.

Table 2 Drive inputs (same characteristics of both motors)

$K_{MS_1} = 0.0081$ N.mA^{-2}
$K_{MS_2} = K_{MS_1}$ N.mA^{-2}
$K_{ES_1} = 0.005$ V.s.A
$K_{ES_2} = K_{ES_1}$ V.s.A
$I_1 = 0.00014$ kg.m^2
$I_2 = I_1$
$U = 24$ V
$M_Z = 0.11$ N.m
$R_1 = 1.19\ \Omega$
$R_2 = R_1$
$L_1 = 0.0098$ H
$L_2 = L_1$
$k_1 = 6782$ N.m.rad^{-1}
$k_2 = k_1$
$b_1 = 0.0022$ N.m.s^{-1}
$b_2 = b_1$

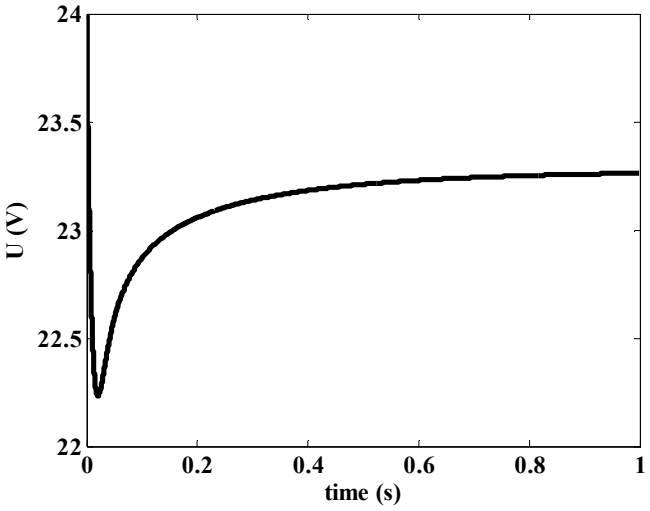

Fig. 5 Power supply voltage changes

The speed-torque characteristic is drawn in Fig. 6 from the beginning of the operation.

The current/time history curve of the first DC motor represents the Fig 7. It depends on the ratio of the armature inductance and the resistance values L, R.

The resultant velocity of the rammer is portrayed in the Fig. 8. It is clear that the rammer acts onto projectile during all period and that it is accelerated to the maximal value.

The coupling between part 1 or 2 and 3 is represented with the spring link in Fig. 9 and they are denoted as M_{13}, M_{23}.

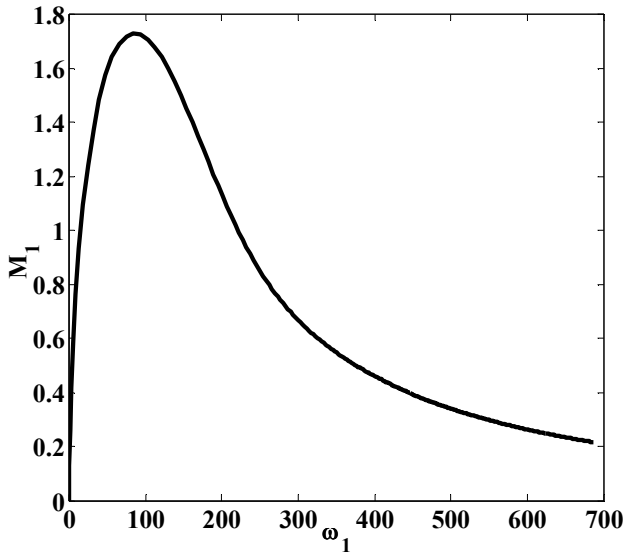

Fig. 6 Speed-torque characteristic

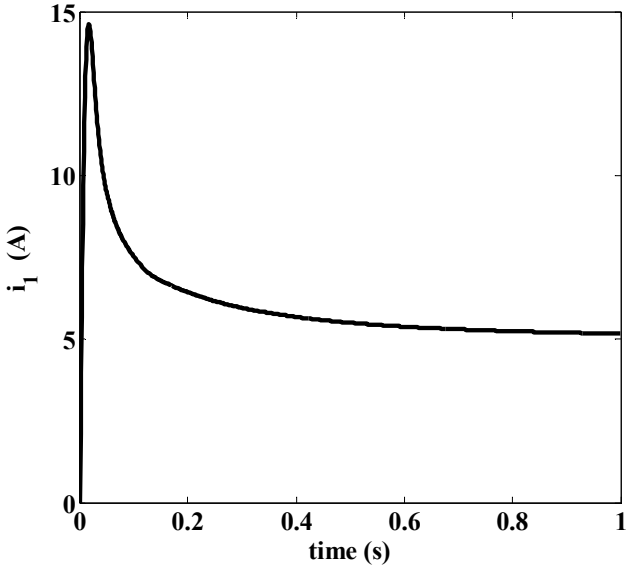

Fig. 7 Current/time history

Both linking moments are same since inputs are same as well and it is the theoretical case. But during service very unusual stages can occur: the different characteristics of drives or malfunctions when one of the motors is excluded from the function and that becomes load of the second one. It is very important to know what happens foremost in military technologies when the system reliability is on the first place.

The influence of the drive different characteristics on the behaviour of the system is explained furthermore.

The drive characteristics have been chosen according to experts group having knowledge and experience in this branch, see Table 3.
The results of this second case are presented next.
The ramming velocity as one of the most important characteristics changes negligible.

Table 3 Drive inputs (different characteristics of both motors)

$K_{MS_1} = 0.0081$ N.mA^{-2}
$K_{MS_2} = 0.0088$ N.mA^{-2}
$K_{ES_1} = 0.005$ V.s.A
$K_{ES_2} = 0.005$ V.s.A
$I_1 = 0.00014$ kg.m^2
$I_2 = I_1$
$I_3 = 0.00017$ kg.m^2
$U = 24$ V
$M_Z = 0.11$ N.m
$R_1 = 1.19\ \Omega$
$R_2 = 1.1\ \Omega$
$L_1 = 0.0107$ H
$L_2 = 0.0098$ H
$k_1 = 6782$ N.m.rad^{-1}
$k_2 = k_1$
$b_1 = 0.0022$ N.m.s^{-1}
$b_2 = b_1$

The course of the 1st motor current $i_{1\ is}$ not too different comparing with Fig. 7. Due to the change of the electromechanical and the time constant the current value at the beginning of the operation is greater but without substantial effect on the final rammer velocity which is necessary to obtain the suitable engraving of the projectile driving band into the forcing cone in the barrel.
Nevertheless the mechanical and electrical system is able to ensure reliable operation at the end of ramming. The greater value at the beginning of the operation achieves the 1st motor and after the transient performance the both motor drive the system with the same torque, see Fig. 10.
At the end of this part the overall exclusion of the motor from the drive due to malfunction has been discussed. The change of the ramming velocity has been studied.

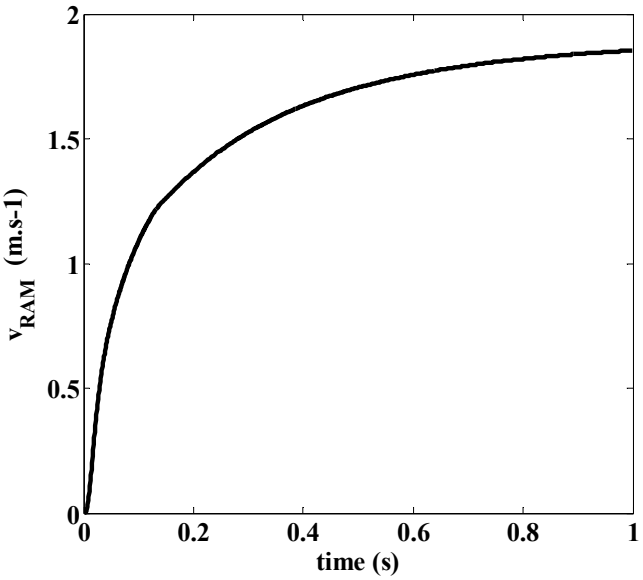

Fig. 8 Rammer velocity

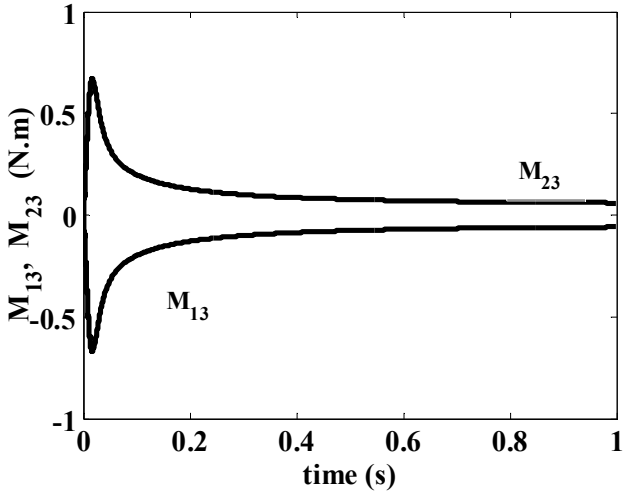

Fig. 9 Elastic links between motors and part 3

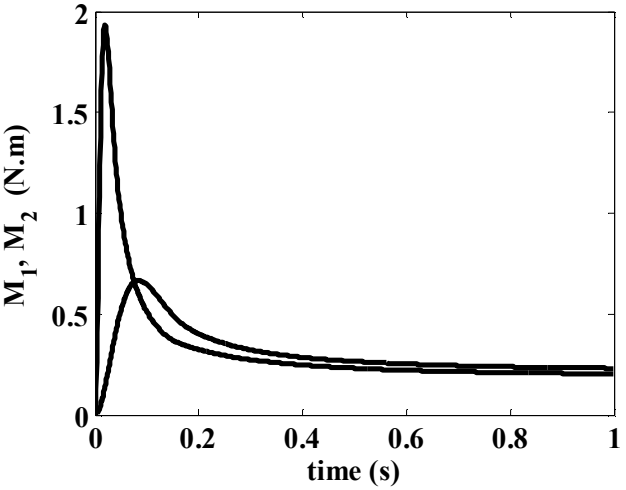

Fig. 10 Motor torques – different characteristics

The non-operating motor is the load for the operating one and it is interesting how the ramming device works.

The maximal ramming velocity attains at 70% of the nominal as it is given in Fig. 11 and the elastic links between motors and part 3 are depicted in Fig. 12.

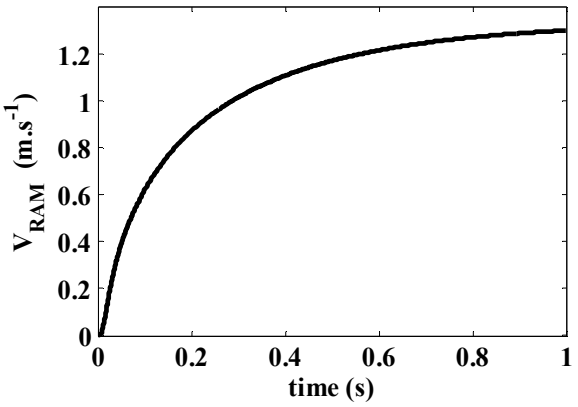

Fig. 11 Ramming velocity – one DC motor out of order

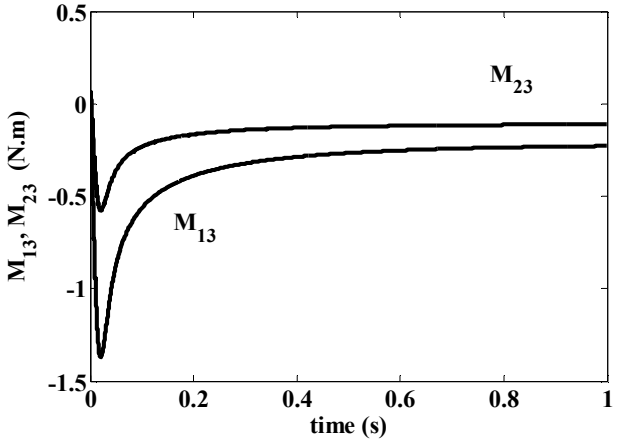

Fig. 12 Elastic links during malfunction of the one motor

During this simulation the maximum electrical power reached the value of 350W.

5 Twin hydraulic drive in chain gun application

The second case will describe the chain gun system which is known in other military area, for example in [2] or [5]. The simplification of this system with the functional diagram is depicted in Fig. 13. Energy is supplied by an electric motor which drives a chain mounted on four sprockets housed in a breech casing. The chain moves with constant speed. Attached to one of its links is a pin, which carries a sliding block. The sliding block moves in a traverse groove in the breech carrier. The chain moves the breech carrier backwards and forwards and provides stationary periods for firing and feeding the cartridge. Firing forces are transmitted to a short barrel extension via the rotating breech bolt. The drive system has none of the firing stressed transmitted to it.

The time taken to complete one cycle is shown on the functional diagram:

$$T = 2\Delta t + t_1 + t_2 + t_3 + t_4 + t_5 + t_6 \quad (18)$$

because

$$t_1 = t_3 = t_4 = t_6 \text{ and } t_2 = t_5$$

then

$$T = 2(\Delta t + t_2 + 2t_1). \quad (19)$$

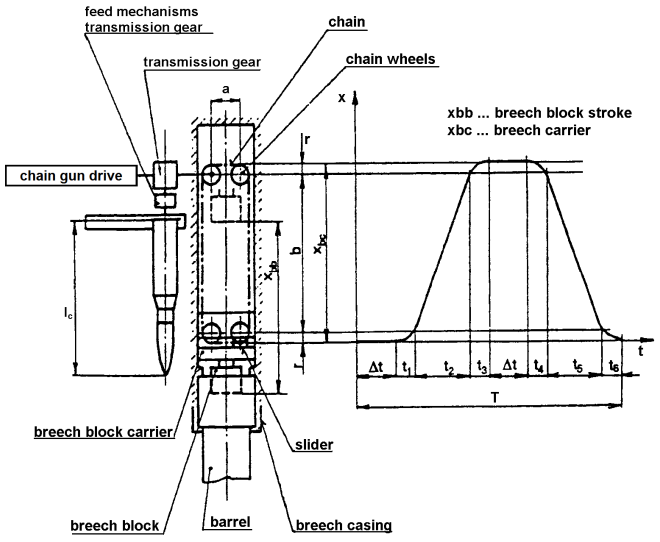

Fig. 13 Chain gun scheme

The advantage of the chain-gun operating mechanism is that the accelerations and velocities are much lower than in conventional operating systems, with no impacts suffered by the working parts. The drive system does not depend on the weapon being fired and so does not stop if there is a cartridge misfire: the misfired cartridge is ejected from the weapon along with the empty cartridge case. The rate of fire can be changed by varying the chain velocity, which is controlled by the electric motor. However, it is necessary to provide an external power source; in the 7.62mm calibre chain-gun the power requirement is 300W. But the required power rises according to the increasing of the calibre and the required rate of fire. The weapons having the 25mm or 30mm calibre demand the 1kW of power and 35mm weapons more when they fire 200rds/min. The increasing of the rate of fire to 500rds/min requires the 8kW of power.

Prior to the dynamic investigation of the chain gun system the kinematic relations have to be solved. The breech block carrier displacement, velocity and acceleration can be established using the Fig. 13.

The parts of the functional diagram are divided into eight sections according to the steer angle φ of the driven chain wheel connecting the chain with the transmission gear. The one period of the reference point motion (that carries the slider for example) is

$$\varphi = \frac{l_r}{r} = \frac{2(a + b + \pi r)}{r} \quad (20)$$

where l_r - chain length,
r - chain wheel radius,
a, b - design dimensions.

The first section after every shot comes on when the time $t \in (0; \Delta t)$: breech block carrier is in the front position and it does not move because breech block is locked. The steer angle is $\varphi = \frac{a}{r}$ and the displacement, velocity and acceleration of the breech block carrier are:

$$x_{nz} = 0,\ v_{nz} = 0,\ a_{nz} = 0. \quad (21)$$

The second section follows when the time $t \in (\Delta t; t_1)$: breech block carrier is accelerated and unlocking of the breech block occurs. The steer angle is $\varphi = \frac{\pi}{2}$ and kinematic characteristics of the breech block carrier are:

$$\begin{aligned} x_{nz} &= r - r\cos[\omega(t - t_0)], \\ v_{nz} &= r\omega\sin[\omega(t - t_0)], \\ a_{nz} &= r\omega^2\cos[\omega(t - t_0)] + r\varepsilon\sin[\omega(t - t_0)]. \end{aligned} \quad (22)$$

The time t_0 is the time at the end of the first section, ω, ε angular velocity and angular acceleration of the chain wheel.

The part, where the whole breech moves backwards and the cartridge case is ejected from the barrel, is the third part. This part belongs to the time interval $t \in (t_1; t_2)$. Then the steer angle is $\varphi = \frac{b}{r}$ and the kinematic values of the breech block carrier are:

$$\begin{aligned} x_{nz} &= r[1 + \omega(t - t_1)], \\ v_{nz} &= r\omega, \\ a_{nz} &= r\varepsilon. \end{aligned} \quad (23)$$

The time t_1 is the time at the end of the second section.

The time interval in the fourth section, when the breech is braked and cartridge case is ejected, is described by the interval $t \in (t_2; t_3)$. The steer angle is

$$\varphi = \frac{\pi}{2},$$

and kinematic values are:

$$\begin{aligned} x_{nz} &= r + b + r\sin[\omega(t - t_2)], \\ v_{nz} &= r\omega\cos[\omega(t - t_2)], \\ a_{nz} &= r\varepsilon\cos[\omega(t - t_2)] - r\omega^2\sin[\omega(t - t_2)]. \end{aligned} \quad (24)$$

The time t_2 is the time at the end of the third section.

The breech does not move in the rear position when the feeding of the new cartridge begins. This position describes the fifth section according to the time interval $t \in (t_3; \Delta t)$. Then the steer angle is as in the first interval $\varphi = \frac{a}{r}$ and its kinematic values are:

$$x_{nz} = x_{nz_3},\ v_{nz} = 0,\ a_{nz} = 0. \quad (25)$$

The breech system is accelerated in the sixth section which is similar to the second part but the velocity has the negative value. The all characteristics are: $\varphi = \frac{\pi}{2}$,

$$\begin{aligned} x_{nz} &= x_{nz3} - r\cos[\omega(t - t_4)], \\ v_{nz} &= -r\omega\sin[\omega(t - t_4)], \\ a_{nz} &= -r\omega^2\cos[\omega(t - t_4)] - r\varepsilon\sin[\omega(t - t_4)]. \end{aligned} \quad (26)$$

The seventh section is described as follows:

$$\begin{aligned} \varphi &= \frac{b}{r}, \\ x_{nz} &= x_{nz_5} - r\omega(t - t_5), \\ v_{nz} &= -r\omega, \\ a_{nz} &= -r\varepsilon. \end{aligned} \quad (27)$$

In addition finally the eighth part can be written $\varphi = \frac{\pi}{2}$,

$$\begin{aligned} x_{nz} &= r\{1 - \sin[\omega(t - t_6)]\}, \\ v_{nz} &= -r\omega\cos[\omega(t - t_6)], \\ a_{nz} &= r\omega^2\sin[\omega(t - t_6)] - r\varepsilon\cos[\omega(t - t_6)]. \end{aligned} \quad (28)$$

The dynamic model is similar to previous case in Fig. 4 where the DC motors are replaced with the hydraulic motors, see Fig. 14. The scheme is simplified without controlling by an electrohydraulic distributor. The engine revolutions are set by means the throttle valves and both motors are driven from the hydraulic source of energy consisting of the pump, bypass valve. The source enables to regulate the pressure (MPa) according to the equation

$$p_G = 25 + 0.8\sin(125t). \quad (29)$$

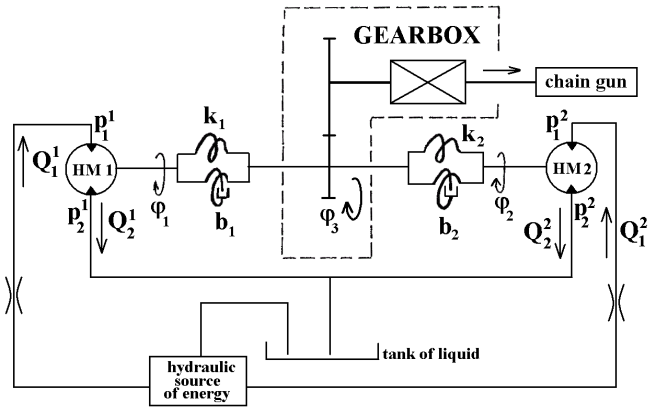

Fig. 14 Dynamic model with hydraulic drives

The mechanical parts are written using the same equations as in the electric drive system, see equations (6), (7) and (8). The hydraulic parts of the drive consist of the four differential equations of the first order for the both motors. Let us note subscript M1 belonging to the first motor and M2 is belonging to the second one. The hydraulic motors torqueses are

$$M_{\mathrm{M1}} = \frac{V_{\mathrm{G_1}}}{2\pi}\left(p_{1,\mathrm{M1}} - p_{2,\mathrm{M1}}\right), \tag{30}$$

$$M_{\mathrm{M2}} = \frac{V_{\mathrm{G_2}}}{2\pi}\left(p_{1,\mathrm{M2}} - p_{2,\mathrm{M2}}\right), \tag{31}$$

where

$V_{\mathrm{G_1}}$, $V_{\mathrm{G_2}}$ are the geometrical volume of the first and the second hydraulic motor.

The input and output pressures are written for the first motor

$$\frac{\mathrm{d}p_{1,\mathrm{M1}}}{\mathrm{d}t} = \frac{(Q_{1,\mathrm{M1}} - \frac{V_{\mathrm{G_1}}}{2\pi}\dot{\varphi}_1 - Z_{1,\mathrm{M1}}\, p_{1,\mathrm{M1}})}{C_1} \tag{32}$$

$$\frac{\mathrm{d}p_{2,\mathrm{M1}}}{\mathrm{d}t} = \frac{(\frac{V_{\mathrm{G_2}}}{2\pi}\dot{\varphi}_1 - Q_{2,\mathrm{M1}} - Z_{2,\mathrm{M1}}\, p_{2,\mathrm{M1}})}{C_2} \tag{33}$$

and for the second one

$$\frac{\mathrm{d}p_{1,\mathrm{M2}}}{\mathrm{d}t} = \frac{(Q_{1,\mathrm{M2}} - \frac{V_{\mathrm{G_1}}}{2\pi}\dot{\varphi}_2 - Z_{1,\mathrm{M2}}\, p_{1,\mathrm{M2}})}{C_1} \tag{34}$$

$$\frac{\mathrm{d}p_{2,\mathrm{M2}}}{\mathrm{d}t} = \frac{(\frac{V_{\mathrm{G_2}}}{2\pi}\dot{\varphi}_2 - Q_{2,\mathrm{M2}} - Z_{2,\mathrm{M2}}\, p_{2,\mathrm{M2}})}{C_2}. \tag{35}$$

The input and output flows of both motors are calculated from the following algebraical equations

$$Q_{1,\mathrm{M1}} = \mathrm{sgn}(p_{\mathrm{G}} - p_{1,\mathrm{M1}})\sqrt{\frac{|p_{\mathrm{G}} - p_{1,\mathrm{M1}}|}{R_1}}, \tag{36}$$

$$Q_{2,\mathrm{M1}} = \mathrm{sgn}(p_{2,\mathrm{M1}} - p_3)\sqrt{\frac{|p_{2,\mathrm{M1}} - p_{1,\mathrm{M1}}|}{R_2}}, \tag{37}$$

$$Q_{1,\mathrm{M2}} = \mathrm{sgn}(p_{\mathrm{G}} - p_{1,\mathrm{M2}})\sqrt{\frac{|p_{\mathrm{G}} - p_{1,\mathrm{M2}}|}{R_1}}, \tag{38}$$

$$Q_{2,\mathrm{M2}} = \mathrm{sgn}(p_{2,\mathrm{M2}} - p_{3,\mathrm{M2}})\sqrt{\frac{|p_{2,\mathrm{M2}} - p_{1,\mathrm{M2}}|}{R_2}}. \tag{39}$$

The parameters used in (30) – (39) are:

p_1 – input pressure,
p_2 – output pressure,
p_{G} – pump pressure, see (29),
p_3 – waste pressure (0.5 MPa),
R_1 – input hydraulic resistance,
R_2 – output hydraulic resistance,
Z_1 – input hydraulic losses,
Z_2 – output hydraulic losses,
C_1 – input hydraulic capacity,
C_2 – output hydraulic capacity.

The hydraulic capacity C generally depends on the liquid volume in the input and output pipe or in the hose and on the liquid volume compressibility factor β which is usually about $6.8\text{x}10^{-10}$ Pa^{-1} and changes according to the air volume in the liquid.

5 Results of chain gun calculations

The main input data used in the calculations are in the Table 4. Due to the case study there are used the same hydraulic parameters which belong to both hydraulic motors and their accessories. In addition to the characteristics are not variable as it is in praxis because the real type of construction is not available. In contradistinction to the previous case the pump pressure changes only due to quality of the source but does not change according to the real flows as it is mentioned in case of the electric drive, see (17). There the supply voltage substantially depends on the armature currents and this source is considered as the soft source. The hydraulic losses Z have not been considered. The motors mass moments of inertia have been determined from the catalogue card which has been disposable, not military configuration with special properties according

to the military standards.

Table 4 Hydraulic drive inputs

$V_{G_1} = 0.00001928\ \mathrm{m}^3$
$V_{G_2} = V_{G_1}$
$C_1 = 5\mathrm{x}10^{-12}\ \mathrm{m}^3\mathrm{Pa}^{-1}$
$C_2 = 7\mathrm{x}10^{-12}\ \mathrm{m}^3\mathrm{Pa}^{-1}$
$I_1 = 0.0079\ \mathrm{kg.m}^2$
$I_2 = I_1$
$I_3 = 0.008\ \mathrm{kg.m}^2$
$M_Z = 0.5\ \mathrm{N.m}$
$R_1 = 7\mathrm{x}10^{12}\ \mathrm{Pa.s}^2.\mathrm{m}^{-6}$
$R_2 = 3.3\mathrm{x}10^{12}\ \mathrm{Pa.s}^2.\mathrm{m}^{-6}$
$k_1 = 6000\ \mathrm{N.m.rad}^{-1}$
$k_2 = k_1$
$b_1 = 0.2\ \mathrm{N.m.s}^{-1}$
$b_2 = b_1$

Several results are shown on Figures 15 - 22.
There are the main characteristics: breech block carrier displacement – Fig. 15, breech block carrier velocity – Fig. 16 and breech block carrier acceleration – Fig. 17. The figures clearly explain the rise of the breech block carrier velocity during acceleration time. It is approximately 0.2s, see Fig 18 as well, and after that time the gun is able to fire with nominal rate of fire.

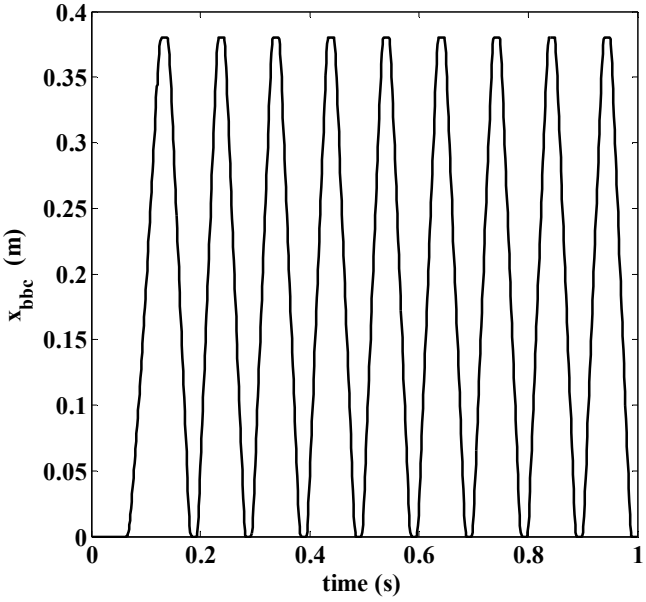

Fig. 15 Breech block carrier displacement

The rate of fire achieves 600 rounds/min in our object in view. The breech block carrier is accelerated to the maximal velocity 10 or 11 m/s which are similar to the automatic cannons using classical drive.

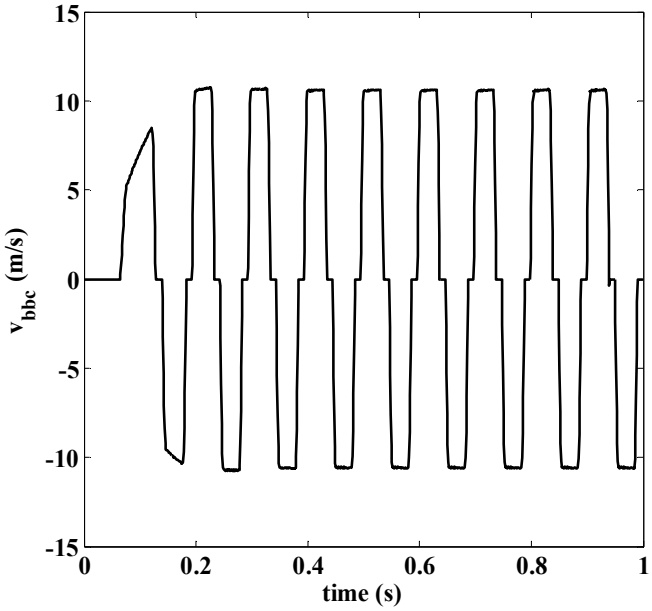

Fig. 16 Breech block carrier velocity

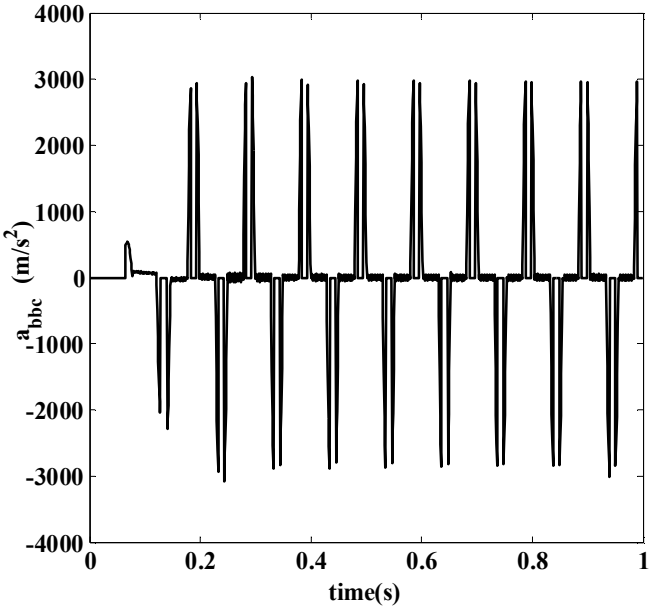

Fig. 17 Breech block carrier acceleration

The course of the acceleration (Fig. 17) shows that these values are much less than the gas or recoil operating systems. It is the main advantage of the chain guns which enables the suitable reliability and operating lifetime.
The chain wheel angular velocity (Fig. 18) changes according to the reduced mass moment of inertia (Fig. 19) how breech mechanism and others operate but in the opposite direction. It means that when reduced mass increases the angular velocity drops and vice versa.

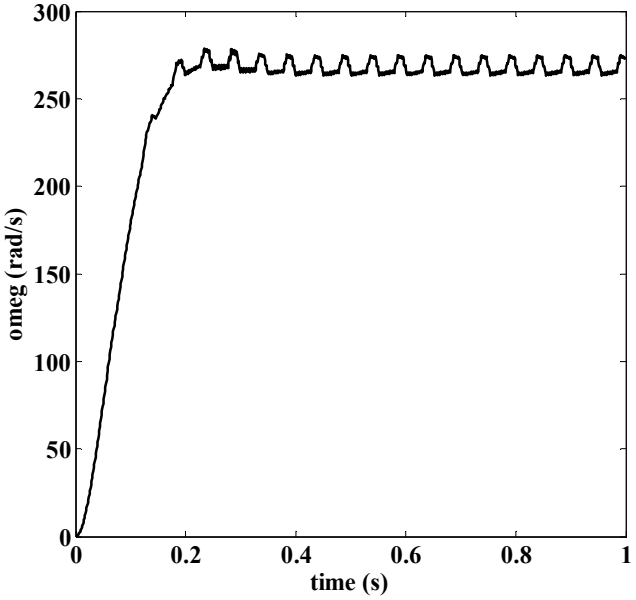

Fig. 18 Chain wheel angular velocity

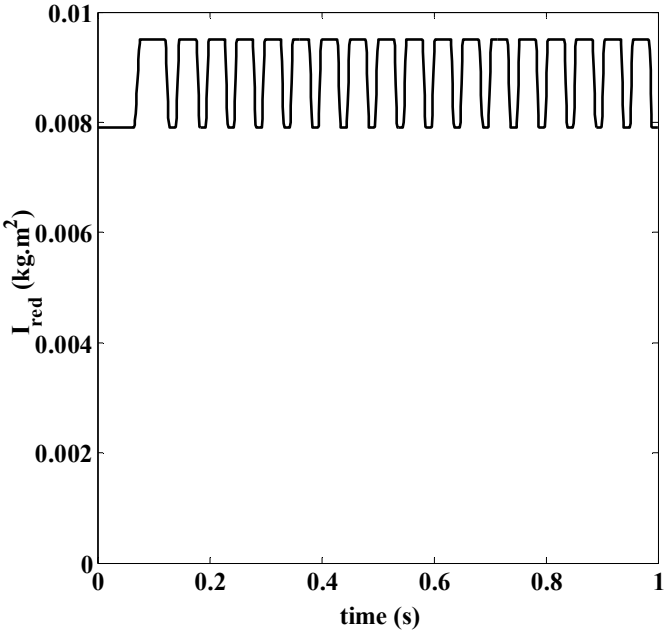

Fig. 19 Reduced mass moment of inertia part 3

The member describing the change of the mass moment of inertia in the equation (8) has been changed so that the derivation could be calculated according to the time and the result is shown in the Fig. 20. Then the component in equation (8) changes into $0.5\frac{\mathrm{d}I_3^{\mathrm{red}}}{\mathrm{d}t}\dot{\varphi}_3$ and the other ones are same. The variation of the inertia mass moment derivation influences behaviour of the weapon mechanism significantly and cannot be neglected, as it is mentioned in [4], [13].

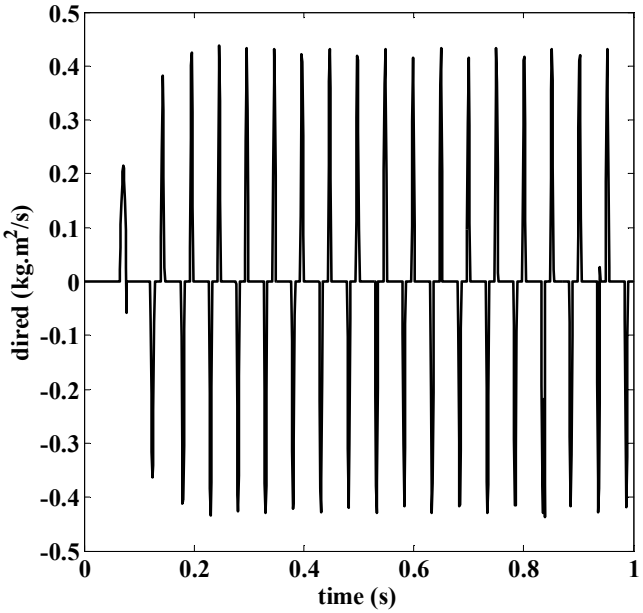

Fig. 20 Reduced mass moment of inertia part 3 derivation

The characteristics describing operation of the hydraulic motors are portrayed right now. The input and output pressures – Fig. 21 – and the input and output flows – Fig. 22 – in one motor show a stabile action after the acceleration of the mechanical system. Only small variations in the input side are caused by the hydraulic source pulsations.

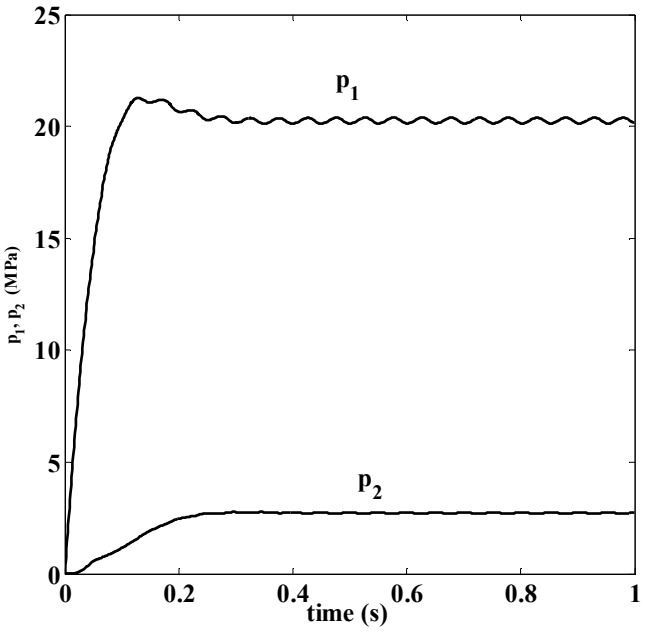

Fig. 21 Input and output pressures in the 1st hydraulic motor

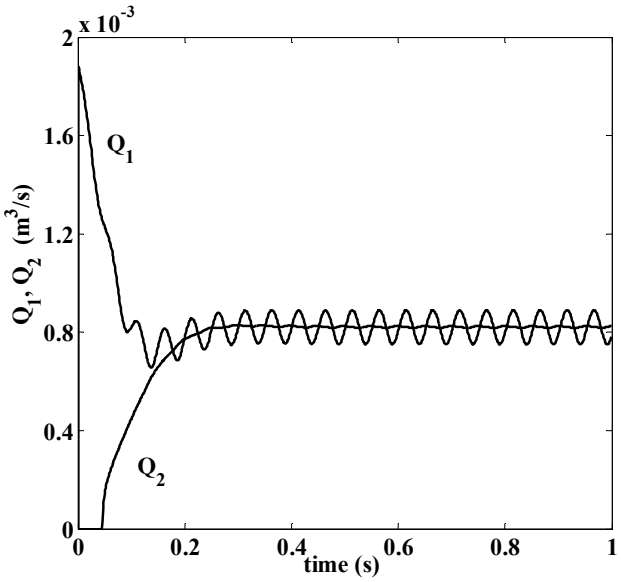

Fig. 22 Input and output flows in the 1st hydraulic motor

6 Conclusion

The results given in the figures reflect a good coincidence with the real piece which was explored according to presented theory. The theory was verified on the other examples of weapons patterns as it is published in references [3] or [7] for example.

The procedure used in this article has been applied in the Czech research institutes and in the University of Defence in Brno as additional teaching material for students of weapons and ammunition branch.

In future it is supposed to study the influence of rammer stiffness (e.g. linking between rammer and projectile will be elastic and system will have over one degrees of freedom) and the influence of the mass change throughout the ramming device operation together with the engraving of the projectile into the forcing cone.

The weapons with external drive will be investigated so that the other resistances could be included into the consideration - extraction force, triggering or more sophisticated feeding device for example.

References:

[1] Allsop, D. F., Balla, J., Cech, V., Popelinsky, L., Prochazka, S., Rosicky, J. *Brassey´s Essential Guide to MILITARY SMALL ARMS*. London, Washington. Brassey´s, 1997.

[2] Allsop, D. F. *Cannons*. London, Washington. Brassey´s, 1995.

[3] Balla, J., Popelinsky, L., Macko, M. *Guns II.* Textbook. Brno: University of Defence. Czech Republic, 2009.

[4] Balla, J., Popelinsky, L, Krist, Z. *Theory of High Rate of Fire Automatic Weapon with Together Bound Barrels and Breeches.* WSEAS Transactions on applied and theoretical mechanics. (Greece), 2010, 5, No. 1, 71-80 p. ISSN: 1991-8747.

[5] Chinn, G. *The Machine Gun*. Volume V. Edwards Brothers Publishing Co., Ann Arbor Michigan, 1987.

[6] *Engineering Design Handbook. Guns Series. Automatic Weapons*. Headquarters, U.S. Army Materiel Command, February, 1970.

[7] Fiser, M. and Popelinsky, L. *Small Arms*. Textbook. Brno: University of Defence, 2007.

[8] Hayes, J., T. *Elements of Ordnance*. A Textbook For Use Of Cadets Of The United States Military Academy. New York. John Wiley & Sons, Inc. London: Chapman & Hall, Limited.

[9] JN Kriel & De Malan. *Measuring some Parameters Relevant to the ballistic Performance of a 155mm Gun System*. Somchem, a Division of Denel (Pty) Ltd. South Africa. In: Proceedings of IIIrd European Guns, Mortars and Ammunition Symposium. Shrivenham: RMCS, UK, September 1996.

[10] Kalous, J. *Program SNAP – A Tool For Electromechanical Drives Analyses.* In: Engeneering MECHANICS, Vol. 16, 2009, No. 4, p. 251 – 264. ISSN 1802 – 1484.

[11] Kunzel, G., Bezouska, V. *The Simulation of Electromechanical Drive with DC Motor*. The Proceedings of the 4th WSEAS International Conference on Power Engineering Systems (ICOPES `05). Rio de Janeiro, Brazil, April 25-27, 2005.

[12] Macko, M. *A simulation of the sport small arms trigger mechanisms*. In 10th WSEAS Int Conf on Math Methods, Computat Tech and Intelligent Syst, Corfu, Greece, October 26-28, 2008.

[13] Pust, L., Kalous, J., Kratochvil, C., Houfek, L., Houfek, M. *Nonlinear vibrations of complex electromechanical systems*. Academy of Science of the Czech Republic Institute of Termomechanics Center of Mechatronics. Prague Czech Republic, 2008.

[14] *Vibration and Shock Handbook*. Edited by Clarence W. de Silva. CRC Press. Taylor & Francis Group. ISBN 0-8493-1580-8.

[15] Vitek, R. *Influence of the small arm barrel bore length on the angle of jump dispersion.* In The Proceedings of the 7th WSEAS International Conference on System Science and Simulation in Engineering, Venice (Italy), November 21 – 23, 2008.

Acknowledgement

The work presented in this paper has been supported by the research projects: VZ FVT 402.